We are IntechOpen,
the world's leading publisher of
Open Access books
Built by scientists, for scientists

6,900
Open access books available

186,000
International authors and editors

200M
Downloads

Our authors are among the

154
Countries delivered to

TOP 1%
most cited scientists

12.2%
Contributors from top 500 universities

CLARIVATE ANALYTICS
BOOK CITATION INDEX
INDEXED

WEB OF SCIENCE™

Selection of our books indexed in the Book Citation Index
in Web of Science™ Core Collection (BKCI)

Interested in publishing with us?
Contact book.department@intechopen.com

Numbers displayed above are based on latest data collected.
For more information visit www.intechopen.com

Dynamic Behavior of Dust Particles in Plasmas

Yoshifumi Saitou and Osamu Ishihara

Abstract

Experimentally observed dynamic behavior, such as a particle circulation under magnetic field, a bow shock formation in an upper stream of an obstacle, etc., will be reviewed. Dust particles confined in a cylindrical glass tube show a dynamic circulation when strong magnetic field is applied from the bottom of the tube using a permanent magnet. The circulation consists of two kinds of motions: one is a toroidal rotation around the tube axis, and the other is a poloidal rotation. Dust particles are blown upward from near the bottom of the tube against the gravity neighborhood of the tube axis. A two-dimensional supersonic flow of dust particles forms a bow shock in front of a needlelike-shaped obstacle when the flow crosses the obstacle. The slower flow passes the obstacle as a laminar flow. A streamline-shaped void where dust particles are not observed is formed around the obstacle.

Keywords: dust flow, dust fluid, bow shock, dynamic circulation, storm in a glass tube

1. Introduction

The natural world is filled with fluids. Fluids present various phenomena such as waves, oscillations, vortices, etc. Scales of such phenomena vary widely. The bow shock formed near the heliopause is in the astrophysical scale, while the Great Red Spot of Jupiter is in the planetary scale, a tornado is in the earth's atmosphere scale, and a swirling tea in a teacup is in the tabletop scale.

It is often observed that collective behavior of individual particles can be regarded as a fluid. A complex plasma, defined as a plasma in which microparticles are embedded in the background of electrons, ions, and neutral particles, provides one of the examples of the case.

In 1986, Ikezi theoretically predicted existence of a crystalized structure with small particles contained in a plasma [1]. It was in 1994 that Hayashi et al., Thomas et al., and Chu et al. separately found in their experiments that charged dust particles formed the crystalized structure in plasmas [2–4]. Since then, research on dusty plasmas has been actively conducted [5–41]. Looking back on the past, Galilei discovered in 1610 that Saturn had "ears." It was found later that the "ears" were a ring or rings by Huygens, Cassini, etc. [42]. Further later in 1856, Maxwell considered the stability of Saturn's ring and concluded that the stable Saturn's ring must consist of independent particles [43]. The interplanetary space is a plasma state dominantly filled by protons brought by the solar wind. Planetary rings like the Saturn's ring is one of the examples that ubiquitously exist in the universe.

Research of complex plasmas including dust particles is unique in a sense that we can chase the motion of individual dust particles by the naked eye using the visible laser light on site without time delay.

In this chapter, experimentally observed dynamic behaviors, such as a circulation of dust particles under magnetic field and a bow shock formation in an upper stream of an obstacle, will be reviewed. A two-dimensional supersonic flow of dust particles forms a bow shock in front of a needlelike-shaped obstacle when the flow passes the obstacle. The slower flow passes the obstacle as a laminar flow. A streamline-shaped void where dust particles are absent is formed around the obstacle. On the other hand, dust particles confined in a cylindrical glass tube show a three-dimensional dynamic circulation when strong enough magnetic field is applied from the bottom of the tube. The circulation consists of two kinds of motions: one is a toroidal rotation around the tube axis, and the other is a poloidal rotation. Dust particles are blown upward from near the bottom of the tube against the gravity around the tube axis.

2. Bow shock formation in two-dimensional dust flow

A NASA's Spitzer Space Telescope observed a shock structure formed in front of the speedster star known as Kappa Cassiopeia in 1994 [44]. The shock is formed near the boundary between a stellar wind and interstellar medium. Another example of a shock wave can be seen around a boundary between a planetary magnetosphere and a stellar wind. These shock waves are similar to a shock excited in front of a bow of a ship cruising fast a water surface and are called a bow shock.

The bow shock is also observable in a supersonic flow of charged dust particles in a complex plasma. In this section, we will look back our experimental work on the bow shock formation [45]. Charged dust particles levitate at height where the gravity and the sheath electrostatic force acting on each particle are balanced in an experimental device on the ground. Therefore, monosized dust particles distribute and flow in an almost two-dimensional plane. An obstacle is placed in the middle of the dust flow just like the star or the planet in the solar wind or the ship on the ocean. The obstacle is a thin needlelike conducting wire and forms a potential barrier against the dust flow. The bow shock is formed when the dust flow interacts with the potential barrier.

2.1 Experimental setup

The schematic of the experimental device Yokohama Complex Plasma Experiment (YCOPEX) is shown in **Figure 1** [46]. Detailed description on the device and experimental setup can be seen in Ref. [45]. The device consists of a glass chamber and a flat metal plate. The size of the metal plate is 800 mm in length (x direction = the main flow direction) and 120 mm in width (y direction). The device is equipped with an up-and-down gate which is electrically controlled from outside. The up-and-down gate separates the plate into two regions: the reservoir of dust particles and the experimental region. A needlelike conducting wire is placed in the experimental region and is used as an obstacle. The potential of the obstacle is floating against the plasma potential here.

The argon gas pressure is 3.6 Pa. To avoid the drag by neutral particles or by ions [45–49], the vacuum pump and the gas feeding are stopped when the pressure reached the set value. Plasma is generated with an rf discharge of 5 W (13.56 MHz). The measured plasma parameters are $n_e \sim 5 \times 10^{14}$ m^{-3}, $T_e \sim 5$ eV. The plasma potential is ~ -30 V.
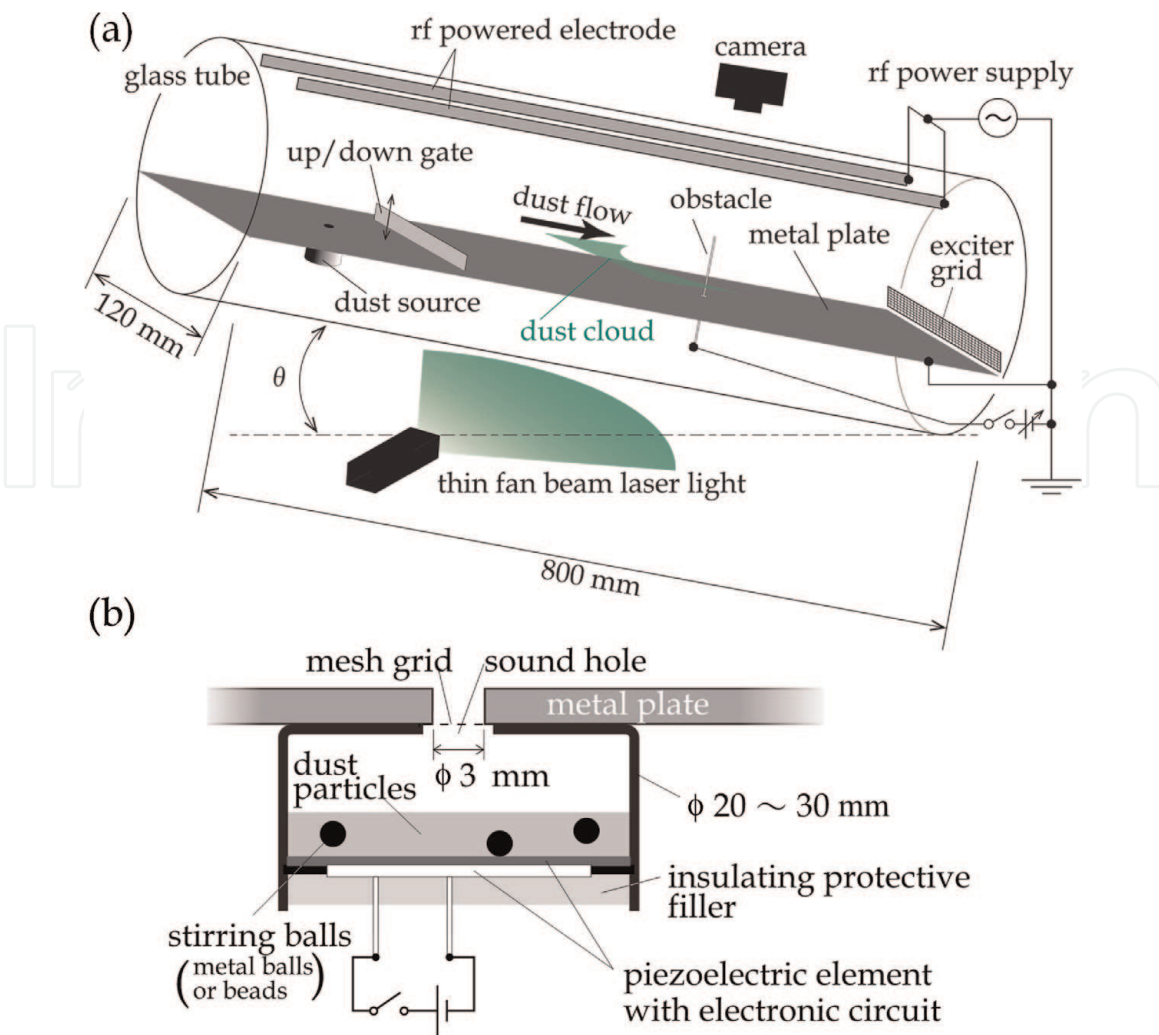
Figure 1.
Schematic drawings of the experimental glass chamber: a YCOPEX device (a) and a piezoelectric buzzer as the dust source (b).

Each dust particle is an Au-coated silica sphere of $a = 5\,\mu m$ in diameter and $m_d = 1.68 \times 10^{-13}$ kg in mass. The particles are charged to $Q = Z_d e = -(4.4 \pm 0.5) \times 10^4 e$, where e is the elementary electric charge [49]. The particles levitate near the boundary between the plasma and the sheath, whose height is approximately 8 mm above the metal plate. The dust particles are irradiated with two thin fan laser lights from the radial directions. Mie-scattered laser light from the particles is observed and recorded with a camera placed outside the device.

In the initial state, the dust particles are accumulated in a cylindrical piezoelectric buzzer which is placed under the metal plate and acts as a dust source. A part of the accumulated dust particles is hopped into the plasma by energizing the buzzer. The dust particles are stored in the reservoir region above the metal plate when the up-and-down gate is in condition to the up position. By tilting the entire device at angle θ and lowering the gate, the stocked dust particles begin moving and form the almost two-dimensional flow. The flow velocity is controlled by changing angle θ. The velocity reaches a terminal velocity before the particles arrive near the obstacle.

2.2 Wave modes observed in a complex plasma

It is known that there are extremely low-frequency longitudinal wave modes in complex plasmas. Typically, one is the dust acoustic (DA) mode, and the other is

the dust lattice (DL) mode. The n-dimensional DA wave velocity, C_{DA}^{nD}, and the DL velocity, C_{DL}, are given by

$$C_d = u(Z_d, m_d) f(\kappa), \tag{1}$$

where $C_d = C_{DA}^{nD}$ or C_{DL}, and

$$u(Z_d, m_d) = \sqrt{\frac{Z_d^2 e^2}{\varepsilon_0 m_d \lambda_{Di}}} \tag{2}$$

with ε_0 the permittivity of free space, λ_{Di}, the ion Debye length. The function $f(\kappa)$ is given by

$$f(\kappa) = \begin{cases} \dfrac{1}{\kappa^{3/2}} & \text{for } C_{DA}^{3D} \\[2ex] \dfrac{1}{\sqrt{2\pi\kappa^2}} & \text{for } C_{DA}^{2D} \\[2ex] \sqrt{\dfrac{4\pi\kappa}{(\kappa^2 + 2\kappa + 2)\exp(-\kappa)}} & \text{for } C_{DL} \ (\kappa \gg 1) \end{cases} , \tag{3}$$

where $\kappa = d/\lambda_{Di}$ with d as the interparticle distance [16, 19, 20]. The distance is given by

$$d = \begin{cases} \dfrac{1}{\left(n_d^{3D}\right)^{1/3}} & \text{for } 3-\text{D dust distribution} \\[2ex] \dfrac{1}{\sqrt{\pi n_d^{2D}}} & \text{for } 2-\text{D dust distribution} \end{cases} , \tag{4}$$

where n_d^{3D} and n_d^{2D} are three- and two-dimensional dust densities, respectively.

The velocity of a wave excited in the dusty plasma, C_d, is measured using the time-of-flight method at $\theta = 0$ degree. The velocity of dust acoustic modes coincides well with the velocity of the dust lattice mode around $\kappa = 3 - 6$. The three-dimensional dust acoustic mode with velocity C_{DA}^{3D} is likely the candidate for the observed mode of the wave although the strict mode identification is still to be determined.

2.3 Bow shock formation

The particles flow from the reservoir region to the obstacle by changing the tilting angle θ. The void which has a streamline-like shape can be seen in the hatched area of **Figure 2**. The void is an area where dust particles are absent. The dust flow near the leading edge of the void is decelerated. The trajectories of dust particles are deflected toward the $\pm y$ direction in front of the void.

The flow velocity, v_f, in the upstream area has a constant value which is mainly determined by a balance of the gravitational force controlled by angle θ and the neutral drag force. The flow is almost uniform, and there is no prominent structure in the upstream area when v_f is small. When v_f increases, an arcuate structure where the intensity of the scattered laser light is enhanced is formed in front of the leading edge of the void. For further increase of v_f, a curvature of the arc becomes larger. The tail of the void is extended with increasing values of v_f.
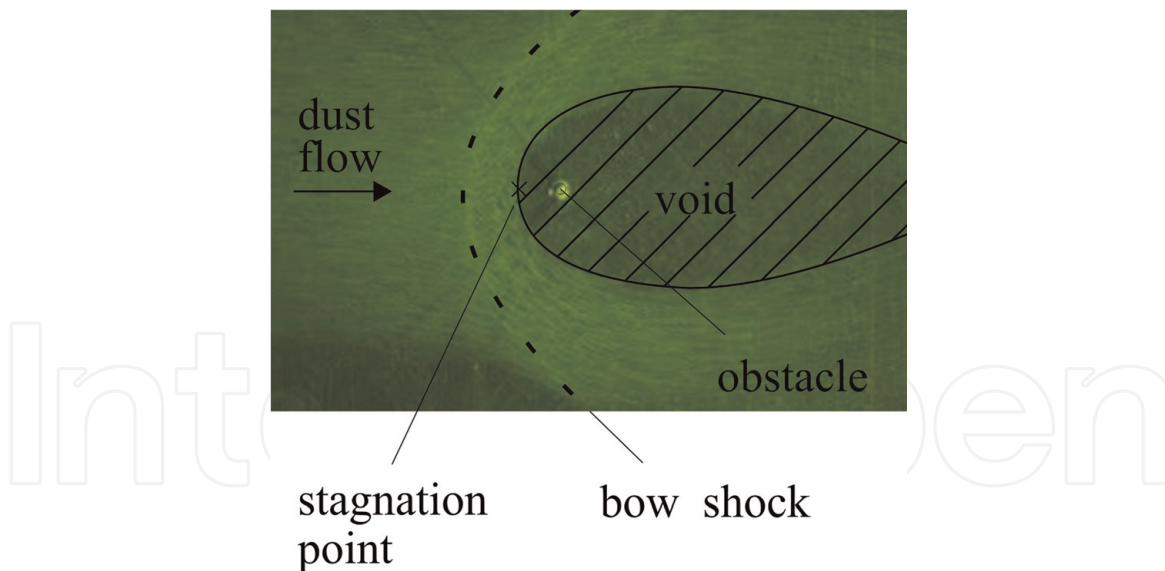
Figure 2.
Typical example of the formed bow shock. Modified from **Figure 3(b)** *of Ref. [45].*

The arcuate structure is the bow shock. The value of v_f is required to exceed Mach number 1 when the bow shock is formed, where the Mach number is defined as the ratio of the flow velocity to the dust acoustic velocity. The experimentally measured velocity is 71 m/s (Mach number $M = 1$). It is found that the arcuate structure is distinctive when the flow is supersonic. In addition, there exists a deceleration region between the leading edge of the arcuate structure and the void as shown in **Figure 2**, that is, there is a region where the flow velocity is reduced in order to keep the flux constant around the obstacle. The presence of such a deceleration region, a subsonic flow region, between the wave front and the stagnation point is one of the defining features of the bow shock [50].

The density ratio n_{dp}/n_{d0} is shown as a function of the Mach number, where n_{dp} is the density in front of the stagnation point and n_{d0} is the density of the upstream area. It is known that a polytropic hydrodynamic model provides criterion for the shock wave formation [50]:

$$\frac{n_{dp}}{n_{d0}} = \begin{cases} \left(1 + \frac{\gamma-1}{2}M^2\right)^{1/(\gamma-1)} & (M < 1) \\ \left(\frac{\gamma+1}{2}\right)^{(\gamma+1)/(\gamma-1)} \frac{M^2}{1 + \frac{\gamma-1}{2}M^2}\left(\gamma - \frac{\gamma-1}{2M^2}\right)^{-1/(\gamma-1)} & (M \geq 1) \end{cases}, \quad (5)$$

where γ is the polytropic index.

2.4 Bow shock by a simulation

A molecular-dynamics simulation code is carried out to examine the bow shock formation. The density ratio n_{dp}/n_{d0} and its spatial distribution are calculated. The simulation result on the density ratio corresponds to the numerical result of Eq. (5) with $\gamma = 2.2$. The experimental result on the density ratio seems to correspond to the case of $\gamma = 5/3$ (= the specific heat ratio of monoatomic gas) ~ 2.2 though there is a small deviation.

The polytropic index found in the simulation and experimental observation may result from the fact that the significant amount of internal energy of the polytropic fluid, which consists of charged dust particles, may be stored in the background

plasma. The value of the complex plasma polytropic index indicates that the present complex plasma is far from isothermal ($\gamma = 1$).

As for the spatial density distribution, the density contour plot shows the arcuate structure, and its curvature increases with increasing Mach number as seen in the experiment.

2.5 Bow shock formation in two-dimensional flow

Under the polytropic process which is a quasi-static process, $p/n^\gamma = const.$ and $T/n^{\gamma-1} = const.$, are held with the polytropic index γ, where p is the pressure, T is the temperature, and n is the density. The polytropic index means

$$\gamma = \begin{cases} 0 & \text{isobaric process} \\ 1 & \text{isothermal process} \\ \kappa_h & \text{isentropic process} \\ \infty & \text{isochoric process} \end{cases} \tag{6}$$

where κ_h is the ratio of specific heat. The experimentally obtained polytropic index lies between 5/3 and 2.2. The value 5/3 is equivalent to the ratio of specific heat of ideal monoatomic gas. The bow shock forms under the almost adiabatic process. The value around 2 is suggested for the investigation on the solar wind [51, 52]. In addition, the dust flow consists of a collection of dust particles with finite size. It is hard to regard the fluid component as ideal. Hence, the polytropic index deviates from 5/3.

The bow shock formation is a nonisothermal process. The pressure ratio and the temperature ratio p_{dp}/p_{d0} and T_{dp}/T_{d0} dependence on the density ratio n_{dp}/n_{d0} are given by $p_{dp}/p_{d0} = (n_{dp}/n_{d0})^\gamma$ and $T_{dp}/T_{d0} = (n_{dp}/n_{d0})^{\gamma-1}$, where p_{dp} and T_{dp} are the pressure and temperature at the stagnation point and p_{d0} and T_{d0} are those at the upstream area, respectively. The results are shown in **Figure 3**. The bow shock is formed for $n_{dp}/n_{d0} > 1$. These results suggest that the polytropic index may be
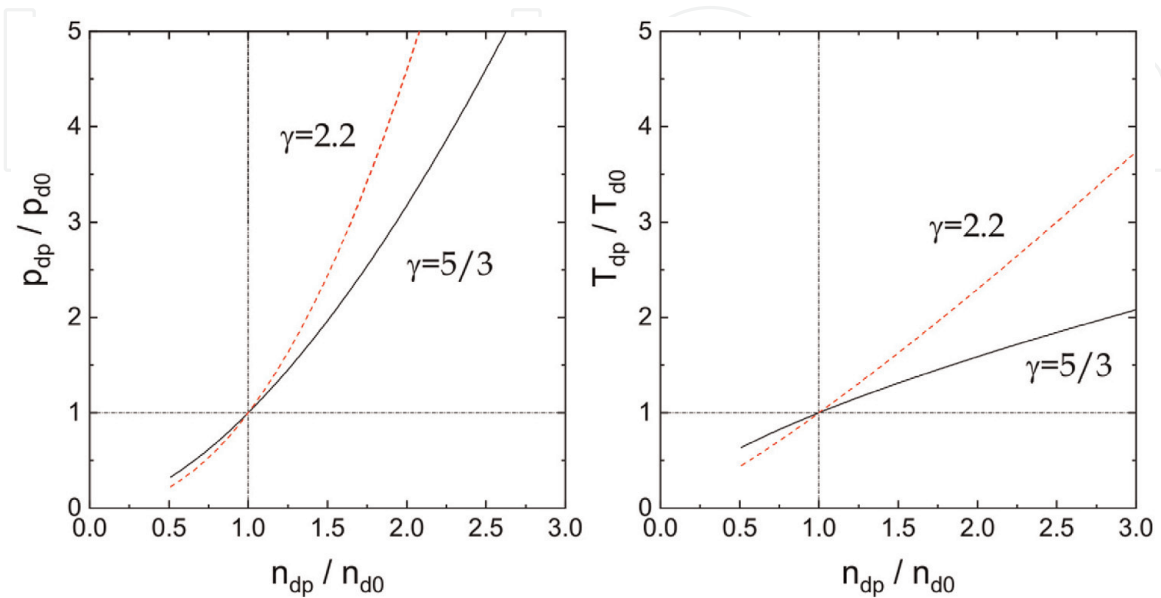

Figure 3.
Expected changes in the ratios of the pressure and the temperature by the bow shock formation $n_{dp}/n_{d0} > 1$ under the polytropic process.

determined by measuring the pressure ratio p_{dp}/p_{d0} or the temperature ratio T_{dp}/T_{d0}.

In this polytropic process, there is a small amount of heat exchange with the outside of the system. The first law of thermodynamics gives

$$dQ = dU + pdV = C_V dT + pdV, \qquad (7)$$

where dQ is a differential heat added to the system, dU is the differential internal energy of the system, and C_V is the specific heat at constant volume. By integrating this equation from state 0 to state 1

$$Q_{01} = C_\gamma (T_1 - T_0), \qquad (8)$$

where $C_\gamma = C_V(\gamma - \kappa)/(\gamma - 1)(>0)$ is the polytropic specific heat. As seen in **Figure 3**, $T_1 - T_0 = T_{dp} - T_{d0} > 0$, and as a result, $Q_{01} > 0$. It is expected that the heat Q_{01} is added to the system for the bow shock formation.

3. Dynamic circulation under magnetic field

You may watch a dynamic motion of tea leaves, set on the bottom of the teacup, by stirring the tea by a teaspoon. The tea leaves get close to the center and rise near the tea surface as illustrated in **Figure 4**. We can see a similar phenomenon in a complex plasma system. In this section, we will look back our experimental work on such a dynamic motion of dust particles in a complex plasma [53].

The observation of particle motion in the dynamic circulation similar to the motion of the tea leaves helps to understand the simple but profound nature of the ubiquitous vortex commonly encountered in nature.

3.1 Experimental setup

The experiment is performed in a cylindrical glass tube as shown in **Figure 5**. Detailed explanation on the experimental setup is given in Ref. [53]. The cylindrical coordinates (r, θ, z) are with the origin at the inner bottom of the tube, and the gravity is in the negative z direction.

The argon gas pressure is $p = 5 - 25$ Pa. A geometry of the gas supply and exhaust system is configured to avoid the neutral drag force acting on the dust
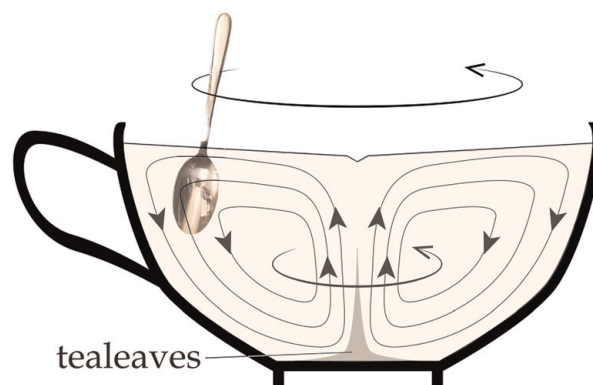

Figure 4.
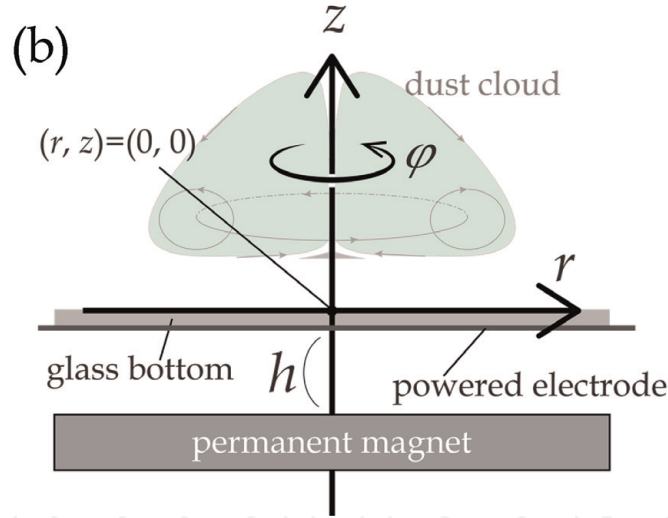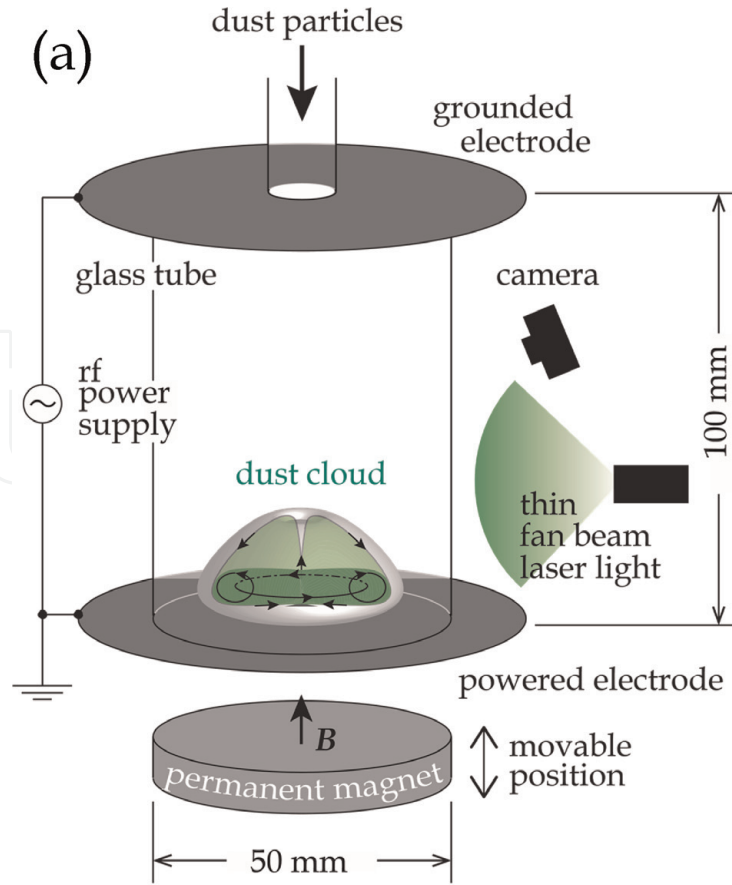*Schematic of tea leaves in tea stirred in a teacup.*

Figure 5.
*Schematic drawing of the experimental glass tube (a) and the coordinate system (b). The structure of the dust cloud can be seen in **Figures 7** and **8**.*

particles in the experimental region. The plasma is produced by an rf discharge of 20 W (13.56 MHz). The electron density is $\sim 10^{14}$ m^{-3}, the electron temperature is ~ 3 eV, and the ion temperature is estimated to be ~ 0.03 eV.

A magnetic field is applied by a cylindrical permanent magnet of 50 mm in diameter placed at a distance h below the powered electrode, and the magnetic field strength is controlled by adjusting the distance h by a jack. The strength of the magnetic field at $r = 0$ is given by

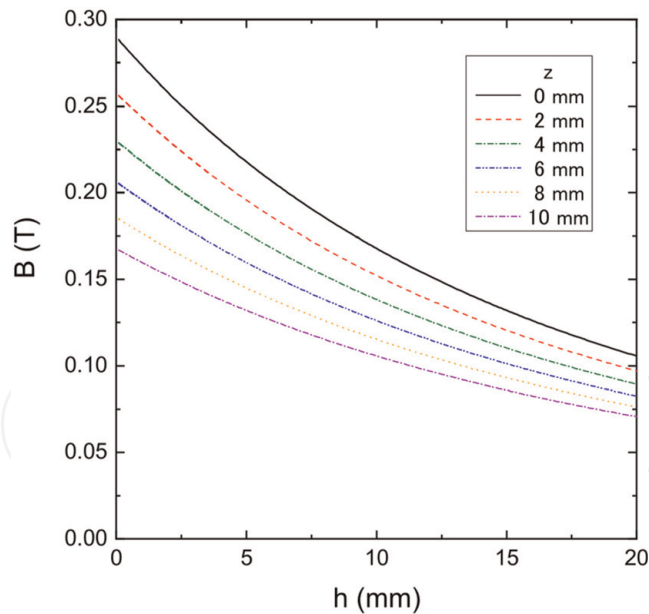$$B(h,z) \approx 0.29 \left(\frac{50}{z + h + 50} \right)^3 \text{ T,} \tag{9}$$

Figure 6.
Strength of the magnetic field at r = 0.

where h and z are measured in mm. The calculated $B(h, z)$ is shown in **Figure 6**.

Dust particles which are acrylic resin spheres of $a = 3$ μm in diameter and $m_d = 1.7 \times 10^{-14}$ kg in mass are supplied from a dust reservoir on the top of the glass tube. Each dust particle is charged in the plasma to $Q \sim -10^4 e$ [49]. The particles in the experimental region are irradiated with a thin fan laser light from the radial directions. The laser sheet can be rotated around the laser axis. The scattered laser light from the particles is observed and recorded with a camera placed outside of the tube.

3.2 Behavior of dust particles in a glass cylinder

Because of the cylindrical symmetry of the glass tube, the motion of dust particles is well observable by watching in a meridional (vertical) plane as shown in **Figures 5, 7**, and **8**.
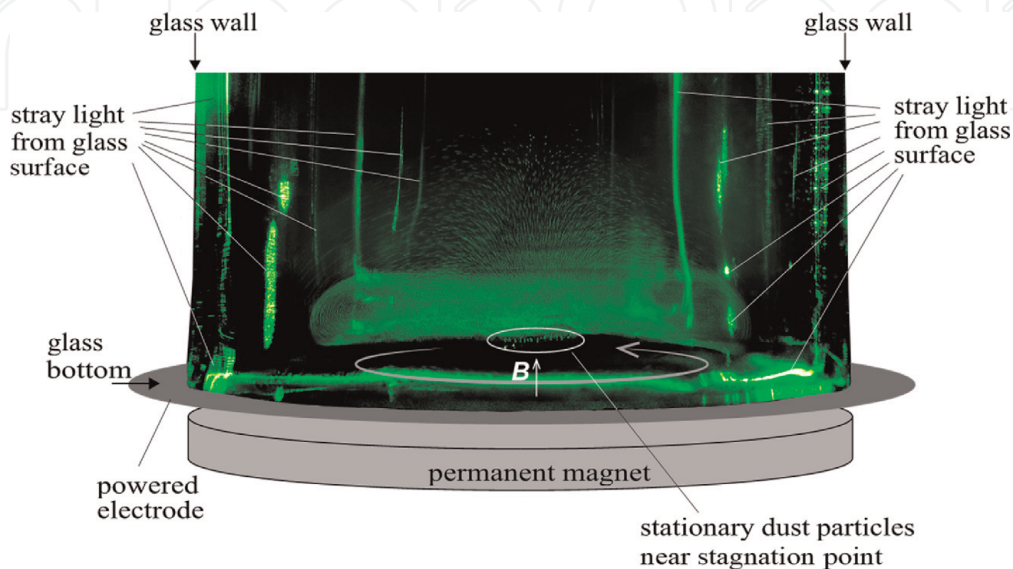

Figure 7.
*Typical example of the formed structure. B = 1.5 kG. Modified from **Figure 2(c)** of Ref. [53]).*
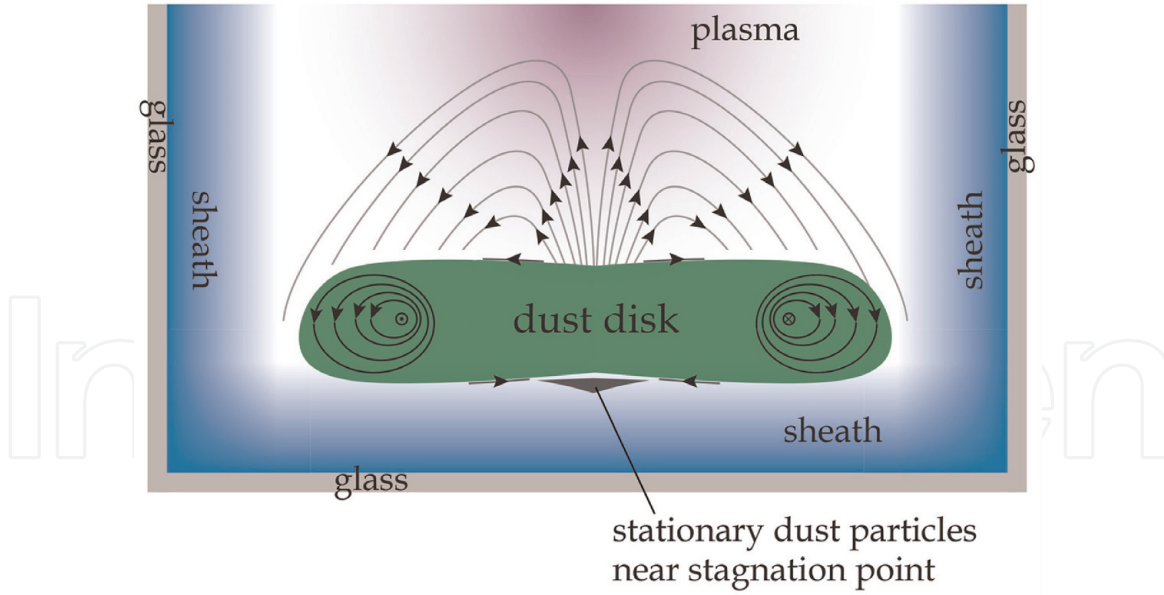
Figure 8.
Schematic of dust particle motion in the meridional plane. The arrows indicate the directions of dust particle motion.

When $B(h \gtrsim 137, z = 0) \lesssim 0.006$ T, the dust particles levitate a few mm above the glass bottom forming a thin disk of radius 20 mm with a dense group of particles at the rim of the disk near the outer wall. When B is increased, the stored dust particles near the wall moved inward to the center and formed a disk of uniformly distributed at $z > 0$. For $B(17, 0) = 0.12$ T with $p = 20$ Pa, where the electrons and ions are weakly magnetized and dust particles are rotating around the axis of the tube. The radial electric field is induced by the ambipolar diffusion and the vertically applied B field produces $E \times B$ drift motion of plasma particles, resulting in a solid body-like azimuthal motion of dust particles with angular velocity $10 - 20$ mm/s.

With a further increase of B and reached $B(12, 0) \approx 0.15$ T, the dust disk becomes the form as shown in **Figure 7**, i.e., the disk is thicker and its radius is smaller. A meridional plane reveals a spectacular movement of dust particles in the thick disk.

Typical trajectories of the spectacular particle motions are shown with arrows in **Figure 8**. There are two small poloidal rotations in the meridional plane near the edges within the thick disk, i.e., one is the clockwise rotation on the right-hand plane, and the other is the counterclockwise rotation on the left-hand plane. The particle motion in the disk as seen in a meridional plane is somewhat similar to the motion of tea leaves as shown in **Figure 4**.

The dust particles move upward against the gravity near $r = 0$. Especially, a part of the particles blows up and exceeds the disk thickness. Such ascending motion of dust particles is followed by radial movement toward the outer wall and then downward. The situation that the particles gush near the top looks like fireworks. After hitting close to the tube bottom, dust particles move inward along the tube bottom. At the same time, dust particles localized near the outer edge of the disk, which do not readily approach $r \approx 0$, form a local circulation in the meridional plane. While dust particles move in these closed circles in a meridional plane, the dust cloud rotates around the z axis and forms a toroidal rotation. As a result, dust particles form a helical motion around the z axis. A schematic illustration of the observed movement of dust particles is something similar as shown in **Figure 4**. In addition, there is a stagnation area around $r \approx 0$ near the tube bottom, where a group of dust particles is not involved in the dynamic meridional rotation as shown in **Figures 4** and **5**.

3.3 MHD dust flow as a rotating fluid

The radial ambipolar diffusion is suppressed due to the electron magnetization, and the current starts to flow in an azimuthal direction in a magnetized plasma. The azimuthal electric field associated with the current density is given by

$$E_\theta = \frac{1}{|\omega_{ce}|\tau_{en}} \frac{\kappa T_e}{e} \frac{1}{n_e} \frac{\partial n_e}{\partial r} \tag{10}$$

In the present case, $E_\theta \approx 9$ V/m because $|\omega_{ce}|\tau_{en} \approx 17$, $\kappa T_e/e \approx 3$ eV, and $(\partial n_e/n_e \partial r)^{-1} \approx 2 \times 10^{-2}$ m, where ω_{ce} is the electron cyclotron angular frequency, τ_{en} is the mean-free-time of the electron-neutral collision, and κ is the Boltzmann constant. This electric field will produce the azimuthal motion of ions with angular velocity $v_{\theta, ion} = eE_\theta/m_i\nu_{in} \approx 40$ m/s. Those ions circling around the tube axis will move dust particles resulting in a dust flow around the axis. Our observed maximum dust angular velocity is $v_{\theta, dust} \approx 0.02$ m/s, near the wall.

The rotating magnetohydrodynamics (MHD) fluid involving dust particles may be described by the Navier-Stokes equation with the continuity equation of an incompressible fluid of constant mass density:

$$\left(\frac{\partial}{\partial t} + \boldsymbol{v} \cdot \nabla\right)\boldsymbol{v} = -\frac{1}{m_d n_d}\nabla p + \nu\nabla^2\boldsymbol{v} + \frac{1}{m_d n_d}\boldsymbol{J} \times \boldsymbol{B} + \boldsymbol{f}, \tag{11}$$

$$\nabla \cdot \boldsymbol{v} = 0, \tag{12}$$

where ν is a kinematic viscosity of the dust fluid and $\boldsymbol{f}\left(=\boldsymbol{f}_g + \boldsymbol{f}_d + \boldsymbol{f}_T + \cdots\right)$ is an external force. The gravitational force $\boldsymbol{f}_g$ is in the negative z direction, while the drag forces $\boldsymbol{f}_d$ by neutral particles, and ions are in the azimuthal direction. The thermophoretic force $\boldsymbol{f}_T$ and the other external forces are negligible in our experimental conditions [54].

We consider rotating fluid with constant angular frequency Ω far from the tube bottom ($z = 0$). Eqs. (11) and (12) can be solved for steady, axisymmetric flow with $\boldsymbol{v} = (v_r, v_\theta, v_z)$ in cylindrical coordinates with boundary conditions $v_\theta = r\Omega$, $v_r = 0$ at $z = \infty$, and $v_r = v_\theta = v_z = 0$ at $z = 0$. We assume $\boldsymbol{J} = (0, J_\theta, 0)$ and $\boldsymbol{B} = (0, 0, B)$. The equilibrium condition requires

$$-r\Omega^2 = \frac{1}{m_d n_d}\left(\frac{\partial p}{\partial r} - J_\theta B\right), \tag{13}$$

indicating that the centrifugal force on a dust particle is balanced by the pressure gradient and the Lorentz force.

By introducing dimensionless parameters, $\bar{v}_r = v_r/r\Omega$, $\bar{v}_\theta = v_\theta/r\Omega$, $\bar{v}_z = v_z/\sqrt{\nu\Omega}$, $\bar{p} = p/\rho\nu\Omega$, and $\bar{g} = g/\sqrt{\nu\Omega^3}$ with $\bar{z} = z/\sqrt{\nu/\Omega}$. Eqs. (11) and (12) can be expressed by a set of three ordinary differential equations:

$$\begin{cases} \dfrac{d^2\bar{v}_r}{d\bar{z}^2} = 1 + \bar{v}_r^2 - \bar{v}_\theta^2 + \bar{v}_z\dfrac{d\bar{v}_r}{d\bar{z}} \\[2mm] \dfrac{d^2\bar{v}_\theta}{d\bar{z}^2} = 2\bar{v}_r\bar{v}_\theta + \dfrac{d\bar{v}_\theta}{d\bar{z}}\bar{v}_z \\[2mm] \dfrac{d\bar{v}_z}{d\bar{z}} = -2\bar{v}_r \end{cases}, \tag{14}$$

supplemented by the pressure gradient equation:

$$\frac{d\overline{p}}{d\overline{z}} = \frac{d^2\overline{v}_z}{d\overline{z}^2} - \overline{v}_z\frac{d\overline{v}_z}{d\overline{z}} - \overline{g}. \tag{15}$$

The set of equations is well studied as similarity solutions for the rotating fluid [55, 56]. The solution shows the presence of a stagnation point at $(r,z) = (0,0)$ and the presence of a thin boundary layer near the bottom where the fluid moves inward. Our observation shows the boundary layer $3\sqrt{\nu/\Omega} \approx 5$ mm.

As Eqs. (11) and (12) show, dust particles drift in the azimuthal direction, and the centrifugal force on a particle is given by $f_C = m_d r(\alpha\Omega)^2$ with α, a constant less than unity. The centrifugal force is balanced by an inward drag force by neutral particles $f_{dn} = C_D\pi a^2 m_n n_n v_r^2/8$, where C_D is a drag coefficient, m_n is a neutral mass, n_n is a neutral density, and $v_r (= \beta r\Omega)$ is a representative radial velocity of dust particles with a constant $\beta < 1$. The balancing equation gives the equilibrium radius as

$$r = \frac{8}{3C_D}\frac{m_d n_d}{m_n n_n}\left(\frac{\alpha}{\beta}\right)^2\frac{a}{2}. \tag{16}$$

Eq. (16) with $\alpha/\beta \approx 0.03$ gives an equilibrium radius of about 0.02 m, which agrees well with our experimental observation.

3.4 Storm in a glass tube

The mechanism of the meridional dust flow is understood in the following way. Initially dust particles are driven by the ion azimuthal motion caused by the radial plasma density gradient in the presence of a strong vertical magnetic field. While the MHD dust fluid forms a rotation around the tube axis, the angular velocity of dust particles near the tube bottom is reduced by the friction from the sheath plasma transition area. The friction reduces the centrifugal force. As a result, the pressure gradient force together with the Lorentz force which remains the same near the bottom generates a radial inward flow of dust particles. Because of the continuity, the radial inward motion will be compensated by an axial upward flow. Dust particles near the bottom ascend along the tube axis, where the sheath electric force pushes charged dust particles upward. When rising dust particles move outside of the sheath, the dust particles feel only the gravitational force. The ascending motion of dust particles near the axis is followed by the outward movement, and then the particles descend.

A circulation with an inward flow at the bottom has been known as a teacup phenomenon [57], also known as Einstein's tea leaves [58]. In 1926, Einstein explained that tea leaves gather in the center of the teacup when the tea is stirred as a result of a secondary, rim-to-center circulation caused by the fluid rubbing against the bottom of the cup. It is indeed observed in our complex plasma experiment that there were some levitated dust particles staying close to the bottom near the center.

4. Discussion: collective behavior of dust particles as a fluid

A complex plasma is a system consisting of electrons, ions, neutral gas particles, and dust particles. The dust particles are macroparticles of nanometers to micrometers in size. In our experiments, monodisperse dust particles of 3 or 5 or 5.6 μm in diameter were used. Behavior of dust particles can be regarded as MHD fluid if $l_{mfp} \ll L$, $\tau_p \gg \tau_d$, and the system keeps quasi-neutrality. Here l_{mfp} is the mean free

path of dust particles, L is a representative scale length of a phenomenon, τ_p is time scale of the evolution of the phenomenon, and τ_d is the dust plasma period [59]. The quasi-neutrality is always kept. Typically, $l_{mfp} \sim 0.1$ mm, $L \sim 1$ cm , $\tau_p \sim 1$ s, and $\tau_d \sim 0.1$ s in our experiments. Hence, the dust cloud can be treated as an MHD fluid.

In water or air or other fluids, a tracer such as aluminum powder or smoke is often used for visualizing a motion of fluid elements. The tea leaves in a teacup are, of course, one of the examples of the tracer as well. This is an indirect observation of the motion because a different tracer has unique characteristics, e.g., a size or a specific weight. The uniqueness comes down to a variation in trackability of the tracer to the fluid element and affects the observation results. The various trackability may give a different result in a measurement. Schlieren imaging and shadowgraph are often used to visualize a flow, too. These methods observe a fluctuation of a density or a refractive index. The setting of the optical system, etc. requires high precision for these methods.

In contrast, in the dust fluid, it is possible to regard each dust particle as a fluid element itself. The particle can be visualized by illuminating using a visible laser light in experiments. The laser light suffers Mie scattering because the size of the dust particle ($\lesssim 10$ μm) is usually larger than the wavelength of the visible laser light ($\sim$ several hundreds nm). The motion of the fluid element is directly visualized without being bothered about both the trackability and the optical precision. It is worth emphasizing that the visualization is achieved on the spot without time lag in experiment.

One of the applications of such a dust fluid is the new method to estimate the dust charge [60]. A dust particle has an electric charge Q in a plasma and levitates at a height where the electrostatic force due to the sheath electric field E and the gravitational force f_g are balancing, $QE = f_g$, on the ground. In experiments to measure the charge of an individual dust particle, it has been hard to separate Q and E independently. In addition, the conventional measurement methods require to change the experimental setup to measure Q and E. However, by regarding the collection of dust particles as a fluid, it is possible to measure the resonant frequency of the dust fluid, i.e., the dust plasma frequency by externally applying the sinusoidal oscillation. The dust charge Q_A is calculated from the resonant frequency. The charge Q_A is an averaged charge for all dust particles present in the experimental region in this case.

In fluid dynamics, the Reynolds number is one of the important parameters. The Reynolds number is given by (inertial forces)/(viscous forces). The Reynolds number is also important in the dust flow. There are investigations relating to the widely changed Reynolds number or the viscosity of dust fluid by the simulation methods [61, 62]. However, it is hard to observe turbulence in our experiments on the dust flow, i.e., it is expected that the Reynolds number is rather small even when $M > 1$.

It is clear that collective behavior of dust particles can be described as a fluid globally. The fluid picture is held where the MHD conditions are satisfied. Intrinsically, however, the dust fluid is a group consisting of independent particles. Therefore, it is expected that the complex plasma includes unique features that is peculiar to a particle system, i.e., properties that are insufficient and difficult to be described by the MHD equation or the Navier–Stokes equation. Such a situation is possible where the MHD conditions do not hold locally. In fact, a few irregular particles are observed in quite rare case. For example, there is a dust particle whose orbit is irregular and different from the others in the way like the dust particle is reflected in a larger angle with faster speed by the obstacle in the bow shock experiment.

In addition, the following experiment may give another example. The schematic of the experimental device is shown in **Figure 9(a)** [63]. The dust cloud exists under an influence of an axisymmetric nonuniform magnetic field applied by a
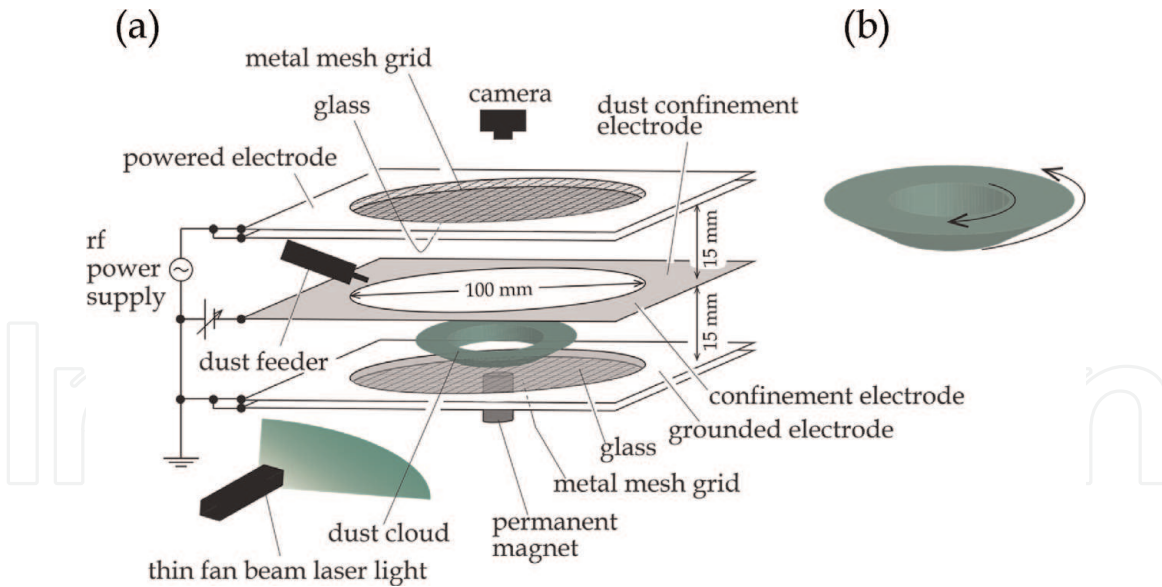
Figure 9.
Schematic of the experimental device (a) and the enhanced illustration of the dust cloud (b). The arrows in (b) are the directions that the particles at the edges rotate. The magnetic field is vertically upward.

small permanent magnet. The dust particles frequently collide with other particles surrounding it. Only the dust particles locate quite near the inner edge and the outer edge rotating along the edges as shown in **Figure 9(b)**. Excluding these edge regions, the collective motion of dust particles seems to be like a fluid. As described in the previous paragraph, the dust fluid has high viscosity. In that case, the rotating particles at the edges have to transfer their momenta to the neighboring particles and must drag the neighbors to their rotating directions. However, in the experiment, the particles do not drag their neighboring particles. It is considered that, at both edges, the dust particles behave as individual particles. Hence, the MHD conditions may be locally broken near the edges, and the particle motion there may suggest one of the particulate-like properties.

5. Summary and subsequent development

It is found in our experiments that the group of dust particles collectively behaves in a similar way to a fluid. In the fast flow of $M > 1$, the bow shock is formed in front of the obstacle. Under the strong magnetic field applied with the permanent magnet, the dust fluid shows a dynamic circulation.

In addition, there is the experimental result which may suggest a particle property of the group of dust particles. It is expected that the dusty plasma or the complex plasma bridges the different nature between continuum mechanics such as fluids and kinetics of particles.

Our results have inspired other researchers in wider fields beyond plasma physics [64–76]. The followings are examples. Tiwari et al. constructed two-dimensional generalized hydrodynamic model and discussed on turbulence in a strongly coupled plasma [64]. They reported that the turbulence was able to occur at a low Reynolds number if the Weissenberg number was high. Kähler et al. derived the ion susceptibility in a partially ionized plasma [65]. Tadsen et al. reported that the dust cloud confined in a magnetized plasma was diamagnetic [66]. Gibson et al. gave an improved understanding of magnetized electron behavior in a dipole magnetic field [67]. Laishram et al. investigated the dust vortex formation in a plasma [68].

Research on dusty plasmas has a strong influence to various areas of physics as seen above. Further progress will be expected.

Acknowledgements

Author details

Yoshifumi Saitou[1]* and Osamu Ishihara[2]

1 School of Engineering, Utsunomiya University, Utsunomiya, Tochigi, Japan

2 Chubu University, Kasugai, Aichi, Japan

*Address all correspondence to: saitou@cc.utsunomiya-u.ac.jp

IntechOpen

References

[1] Ikezi H. Coulomb solid of small particles in plasmas. Physics of Fluids. 1986;**29**:1764

[2] Hayashi Y, Tachibana K. Observation of coulomb-crystal formation from carbon particles grown. Japanese Journal of Applied Physics. 1994;**33**:L804

[3] Thomas H, Morfill GE, Demmel V, Goree J, Feuerbacher B, Möhlmann D. Plasma crystal: Coulomb crystallization in a dusty plasma. Physical Review Letters. 1994;**73**:652

[4] Chu JH, Lin I. Direct observation of Coulomb crystals and liquids in strongly coupled rf dusty plasmas. Physical Review Letters. 1994;**72**:4009

[5] Nosenko V, Goree J, Ma ZW, Piel A. Observation of shear-wave Mach cones in a 2D dusty-plasma crystal. Physical Review Letters. 2002;**88**:135001

[6] Samsonov D, Goree J, Thomas HM, Morfill GE. Mach cone shocks in a two-dimensional Yukawa solid using a complex plasma. Physical Review E. 2000;**61**:5557

[7] Havnes O, Li F, Melansø F, Aslaksen T, Hartquist TW, Morfill GE, et al. Diagnostic of dusty plasma conditions by the observation of Mach cones caused by dust acoustic waves. Journal of Vacuum Science and Technology A. 1996;**14**:525

[8] Melzer A, Nunomura S, Samsonov D, Ma ZW, Goree J. Laser-excited Mach cones in a dusty plasma crystal. Physical Review E. 2000;**62**:4162

[9] Gosh S. Shock wave in a two-dimensional dusty plasma crystal. Physics of Plasmas. 2009;**16**:103701

[10] Luo Q-Z, D'Angelo N, Merlino RL. Experimental study of shock formation in a dusty plasma. Physics of Plasmas. 1999;**6**:3455

[11] Nosenko V, Zhdanov S, Morfill GE. Supersonic dislocations observed in a plasma crystal. Physical Review Letters. 2007;**99**:025002

[12] Ness NF, Scearce CS, Seek JB. Initial results of the imp 1 magnetic field experiment. Journal of Geophysical Research. 1964;**69**:3531

[13] Morfill GE, Thomas HM, Konopka U, Rothermel H, Zuzic M, Ivlev A, et al. Condensed plasmas under microgravity. Physical Review Letters. 1999;**83**:1598

[14] Vladimirov SV, Tsytovich VN, Morfill GE. Stability of dust voids. Physics of Plasmas. 2005;**12**:052117

[15] Thomas E Jr, Avinash K, Merlino RL. Probe induced voids in a dusty plasma. Physics of Plasmas. 2004;**11**:1770

[16] Thompson CO, D'Angelo N, Merlino RL. The interaction of stationary and moving objects with dusty plasmas. Physics of Plasmas. 1999;**6**:1421

[17] Ishihara O. Complex plasma: Dusts in plasma. Journal of Physics D. 2007;**40**:R121

[18] Morfill GE, Ivlev A. Complex plasmas: An interdisciplinary research field. Reviews of Modern Physics. 2009;**81**:1353

[19] Kalman GJ, Hartmann P, Donkó Z, Rosenberg M. Two-dimensional Yukawa liquids: Correlation and dynamics. Physical Review Letters. 2004;**92**:065001

[20] Donkó Z, Kalman GJ, Hartmann P. Dynamical correlations and collective

excitations of Yukawa liquids. Journal of Physics, Condensed Matter. 2008;**20**: 413101

[21] Yeo LY, Friend JR, Arifin DR. Electric tempest in a teacup: The tea leaf analogy to microfluidic blood plasma separation. Applied Physics Letters. 2006;**89**:103516

[22] Arfin DR, Yeo LY, Fried JR. Microfluidic blood plasma separation via bulk electrohydrodynamic flows. Biomicrofluidics. 2007;**1**:014103

[23] Melzer A, Trottenberg T, Piel A. Experimental determination of the charge on dust particles forming Coulomb lattices. Physics Letters A. 1994;**191**:301

[24] Smith BA, Soderblom L, Batson R, Bridges P, Inge J, Masursky H, et al. A new look at the Saturn system: The Voyager 2 images. Science. 1982;**215**:504

[25] Ishihara O. Complex plasma research under extreme conditions. In: Mendonça JT, Resendes DP, Shukla PK, editors. Multifacets of Dusty Plasmas. AIP Conference Proceedings. Vol. 1041. Melville, NY: AIP; 2008. pp. 139-142

[26] Tsytovich VN, Morfill G, Vladimirov SV, Thomas H. Elementary Physics of Complex Plasmas. Heidelberg: Springer; 2008

[27] Piel A. Plasma Physics: An Introduction to Laboratory, Space, and Fusion Plasmas. Dordrecht: Springer; 2010

[28] Ishihara O. Low-dimensional structures in a complex cryogenic plasma. Plasma Physics and Controlled Fusion. 2012;**54**:124020

[29] Nebbat E, Annou R. On vortex dust structures in magnetized dusty plasmas. Physics of Plasmas. 2010;**17**:093702

[30] Tsytovich VN, Gusein-zade NG. Nonlinear screening of dust grains and

structurization of dusty plasma. Plasma Physics Reports. 2013;**39**:515

[31] Kamimura T, Suga Y, Ishihara O. Configurations of Coulomb clusters in plasma. Physics of Plasmas. 2007;**14**: 123706

[32] Kamimura T, Ishihara O. Coulomb double helical structure. Physical Review E. 2012;**85**:016406

[33] Schwabe M, Rubin-Zuzic M, Zhdanov S, Ivlev AV, Thomas HM, Morfill GE. Formation of bubbles, blobs, and surface cusps in complex plasmas. Physical Review Letters. 2009;**102**: 255005

[34] Saitou Y, Ishihara O. Tempest in a glass tube: A helical vortex formation in a complex plasma. Journal of Plasma Physics. 2014;**80**:869

[35] Thomas E Jr, Merlino RL, Rosenberg M. Magnetized dusty plasmas: the next frontier for complex plasma research. Plasma Physics and Controlled Fusion. 2012;**54**:124034

[36] Konopka U, Samsonov D, Ivlev AV, Goree J, Steinberg V, Morfill GE. Rigid and differential plasma crystal rotation induced by magnetic fields. Physical Review E. 2000;**61**:1890

[37] Sato N, Uchida G, Kaneko T, Shimizu S, Iizuka S. Dynamics of fine particles in magnetized plasmas. Physics of Plasmas. 2001;**8**:1786

[38] Ishihara O, Kamimura T, Hirose KI, Sato N. Rotation of a two-dimensional Coulomb cluster in a magnetic field. Physical Review E. 2002;**66**:046406

[39] Ishihara O, Sato N. On the rotation of a dust particulate in an ion flow in a magnetic field. IEEE Transactions on Plasma Science. 2001;**29**:179

[40] Tsytovich VN, Sato N, Morfill GE. Note on the charging and spinning of

dust particles in complex plasmas in a strong magnetic field. New Journal of Physics. 2003;**5**:43

[41] Hutchinson H. Spin stability of asymmetrically charged plasma dust. New Journal of Physics. 2004;**6**:43

[42] Seal D. Jet Propulsion Laboratory [Internet]. 2019. Available from: https://web.archive.org/web/20090321071339/http://www2.jpl.nasa.gov/saturn/back.html

[43] Maxwell JC. On the stability of the motion of Saturn's rings: An essay, which obtained the Adams prize for the year 1856. London: University of Cambridge, Macmillan and Co.; 1859

[44] Spitzer Telescope [Internet]. 2019. Available from: https://www.nasa.gov/jpl/spitzer/bow-shock-wave-20140220

[45] Saitou Y, Nakamura Y, Kamimura T, Ishihara O. Bow shock formation in a complex plasma. Physical Review Letters. 2012;**108**:065004

[46] Nakamura Y, Ishihara O. A complex plasma device of large surface area. The Review of Scientific Instruments. 2008;**79**: 033504

[47] Epstein PS. On the Resistance experienced by spheres in their motion through gases. Physics Review. 1924;**23**:710

[48] Shukla PK, Mamun AA. Introduction to Dusty Plasma Physics. London: Institute of Physics Publishing Ltd.; 2002. Chap. 3, p. 70

[49] Nakamura Y, Ishihara O. Measurements of electric charge and screening length of microparticles in a plasma sheath. Physics of Plasmas. 2009;**16**:043704

[50] Landau LD, Lifshitz EM. Fluid Mechanics. Oxford: Butterworth-Heinemann; 2002. Chaps. 9, 12, and 13, pp. 313-360 and 435-483

[51] Newbury JA, Russel CT, Lindsay GM. Solar wind polytropic index in the vicinity of stream interactions. Geophysical Research Letters. 1997;**24**:1431

[52] Roussev II, Gombosi TI, Sokolov IV, Velli M, Manchester W IV, Dezeeuw DL, et al. A three-dimensional model of the solar wind incorporating solar magnetogram observations. The Astrophysical Journal. 2003;**595**:L57

[53] Saitou Y, Ishihara O. Dynamic circulation in a complex plasma. Physical Review Letters. 2013;**111**: 185003

[54] Ishihara O. Polygon structure of plasma crystals. Physics of Plasmas. 1998;**5**:357

[55] Greenspan HP. The Theory of Rotating Fluids. Cambridge, England: Cambridge University Press; 1968. Chap. 3, pp. 133-184

[56] Tritton DJ. Physical Fluid Dynamics, 2nd ed. Oxford: Clarendon Press; 2011. Chap. 16, pp. 215-242

[57] Maxworthy T. A Storm in a Teacup. Journal of Applied Mechanics. 1968;**35**: 836

[58] Einstein A. Ursache der Mäanderbildung der Flussläufe und des sogenannten Baerschen Gesetzes. Naturwissenschaften. 1926;**14**:223

[59] Landau LD, Lifshitz EM, Pitaevskii LP. Electrodynamics of Continuous Media. Oxford: Butterworth-Heinemann; 2000. Chap. 8, pp. 225-256

[60] Saitou Y. A simple method of dust charge estimation using an externally applied oscillating electric field. Physics of Plasmas. 2018;**25**:073701

[61] Saigo T, Hamaguchi S. Shear viscosity of strongly coupled Yukawa

systems. Physics of Plasmas. 2002;**9**: 1210

[62] Laishram M, Zhu P. Structural transition of vortices to nonlinear regimes in a dusty plasma. Physics of Plasmas. 2018;**25**:103701

[63] Saitou Y. Motions of dust particles in a complex plasma with an axisymmetric nonuniform magnetic field. Physics of Plasmas. 2016;**23**: 013709

[64] Tiwari SK, Dharodi VS, Das A, Patel BG. Turbulence in strongly coupled dusty plasmas using generalized hydrodynamic description. Physics of Plasmas. 2015;**22**:023710

[65] Kähler H, Joost JP, Ludwig P, Bonitz M. Streaming complex plasmas: Ion susceptibility for a partially ionized plasma in parallel electric and magnetic fields. Contributions to Plasma Physics. 2016;**56**:204

[66] Tadsen B, Greiner F, Piel A. Probing a dusty magnetized plasma with self-excited dust-density waves. Physical Review E. 2018;**97**:033203

[67] Gibson J, Coppins M. Theory of electron density in a collisionless plasma in the vicinity of a magnetic dipole. Physics of Plasmas. 2018;**25**:112103

[68] Laishram M, Sharma D, Kaw PK. Analytic structure of a drag-driven confined dust vortex flow in plasma. Physical Review E. 2015;**91**:063110

[69] Kaur M, Bose S, Chattopadhyay PK, Sharma D, Ghosh J. Observation of dust torus with poloidal rotation in direct current glow discharge plasma. Physics of Plasmas. 2015;**22**:033703

[70] Deka T, Bouruah A, Sharma SK, Bailing H. Observation of self-excited dust acoustic wave in dusty plasma with nanometer size dust grains. Physics of Plasmas. 2017;**24**:093706

[71] Meyer JK, Merlino R. Transient bow shock around a cylinder in a supersonic dusty plasma. Physics of Plasmas. 2013;**20**:074501

[72] Jaiswal S, Bandyopadhyay P, Sen A. Experimental observation of precursor solitons in a flowing complex plasma. Physical Review E. 2016;**93**:041201(R)

[73] Ludwig P, Miloch WJ, Kählert H, Bonitz M. On the wake structure in streaming complex plasmas. New Journal of Physics. 2012;**14**:053016

[74] Wilms J, Reichstein T, Piel A. Experimental observation of crystalline particle flows in toroidal dust clouds. Physics of Plasmas. 2015;**22**:063701

[75] Vladimirov SV, Ishihara O. Electromagnetic wave band structure due to surface plasmon resonances in a complex plasma. Physical Review E. 2016;**94**:013202

[76] Sakakibara N, Matsubayashi Y, Iyo T, Terashima K. Formation of pseudo-microgravity environment for dusty plasmas in supercritical carbon dioxide. Physics of Plasmas. 2018;**25**: 010704